ACS APPLIED MATERIALS & INTERFACES

Research Article

www.acsami.org

Threshold-Voltage Shifts in Organic Transistors Due to Self-Assembled Monolayers at the Dielectric: Evidence for Electronic Coupling and Dipolar Effects

Mahdieh Aghamohammadi,[†] Reinhold Rödel,[†] Ute Zschieschang,[†] Carmen Ocal,[‡] Hans Boschker,[†] R. Thomas Weitz,[§,∥] Esther Barrena,*[,‡] and Hagen Klauk*[,†]

[†]Max Planck Institute for Solid State Research, Heisenbergstr.1, 70569, Stuttgart, Germany

[‡]Instituto de Ciencia de Materiales de Barcelona (ICMAB-CSIC), Campus de la UAB, 08193 Bellaterra, Spain

[§]BASF SE, GVE/T − J542s, 67056 Ludwigshafen, Germany

[∥]Innovation Lab GmbH, Speyerer Str. 4, 69115 Heidelberg, Germany

Supporting Information

ABSTRACT: The mechanisms behind the threshold-voltage shift in organic transistors due to functionalizing of the gate dielectric with self-assembled monolayers (SAMs) are still under debate. We address the mechanisms by which SAMs determine the threshold voltage, by analyzing whether the threshold voltage depends on the gate-dielectric capacitance. We have investigated transistors based on five oxide thicknesses and two SAMs with rather diverse chemical properties, using the benchmark organic semiconductor dinaphtho[2,3-b:2′,3′-*f*]thieno[3,2-*b*]thiophene. Unlike several previous studies, we have found that the dependence of the threshold voltage on the gate-dielectric capacitance is completely different for the two SAMs. In transistors with an alkyl SAM, the threshold voltage does not depend on the gate-dielectric capacitance and is determined mainly by the dipolar character of the SAM, whereas in transistors with a fluoroalkyl SAM the threshold voltages exhibit a linear dependence on the inverse of the gate-dielectric capacitance. Kelvin probe force microscopy measurements indicate this behavior is attributed to an electronic coupling between the fluoroalkyl SAM and the organic semiconductor.

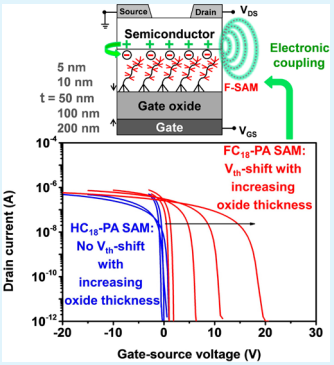

KEYWORDS: *organic transistors, self-assembled monolayers, Kelvin probe force microscopy, gate-dielectric capacitance, threshold-voltage shift*

1. INTRODUCTION

Substantial improvements in the performance and stability of organic thin-film transistors (TFTs) have made them a potential choice for flexible, large-area electronic and optoelectronic applications. A robust way of enhancing the electrical characteristics of bottom-gate organic TFTs is the chemical modification of the interface between the gate oxide and the organic semiconductor thin film by a self-assembled monolayer (SAM). It has been shown that the passivation of the gate-oxide surface with a highly ordered SAM can significantly reduce the density of charge traps at the oxide/SAM interface and thereby provide an enhancement of the charge-carrier field-effect mobility for both p-channel[1] and n-channel organic TFTs.[2] The beneficial effects of the passivation of the gate oxide with a SAM in organic TFTs have been reported for a variety of oxides, including SiO_2,[3−6] Al_2O_3,[7,8] HfO_2,[9−12] ZrO_2,[13−15] $ZrTiO_x$,[16] and TiO_2,[17] and for a variety of SAMs, most notably alkylsilane SAMs[4,18] and alkylphosphonic acid SAMs.[19−21] Enhanced field-effect mobility has also been associated with improvements in the thin-film morphology of the organic semiconductor layer, presumably induced by the surface energy of the SAM-functionalized oxide surfaces.[5]

Another important aspect of functionalizing the gate-oxide surface of organic TFTs with a SAM is the modification of the threshold voltage of the transistors over a range of a few volts to several tens of volts. Kobayashi et al. were among the first to introduce this effect by using various SAMs on a SiO_2 gate dielectric in combination with pentacene and C_{60} as the semiconductors in p-channel and n-channel organic TFTs.[22] In a similar study, Pernstich et al. showed that functionalizing the SiO_2 gate dielectric with different SAMs induces different threshold voltages in pentacene-based TFTs.[23] The physical mechanism responsible for this phenomenon has been under debate, and different explanations have been suggested.

Kobayashi et al. proposed that the threshold-voltage shift is related to the dipolar character of the SAM molecules, arguing that the built-in electric field of the SAM is compensated by the electric field externally applied across the gate dielectric. The electric field inside the SAM is expressed as the electrostatic potential difference across the SAM divided by its thickness

Received: March 30, 2015
Accepted: September 28, 2015
Published: September 28, 2015

DOI: 10.1021/acsami.5b02747
ACS Appl. Mater. Interfaces 2015, 7, 22775−22785

($E_{SAM} = V_{SAM}/t_{SAM}$), with V_{SAM} given by the Helmholtz equation:

$$V_{SAM} = \frac{N_{SAM} P_z}{\varepsilon_0 \varepsilon_{SAM}} \quad (1)$$

where N_{SAM} is the molecular density of the SAM (the number of molecules per unit area), P_z is the perpendicular component of the dipole moment of the SAM, ε_0 is the vacuum permittivity, and ε_{SAM} is the relative permittivity of the SAM. Following this line of argumentation, and assuming that the density of the dipole-induced charges accumulated at the semiconductor−dielectric interface is given by $Q_{SAM} = V_{SAM}C_{SAM}$, a general relation between the electrostatic potential of the SAM and the SAM-induced change in the threshold voltage (V_{th}) has been proposed:[23−26]

$$V_{th} = -\frac{C_{SAM} V_{SAM}}{C_{diel}} + \varphi \quad (2)$$

with C_{diel} being the capacitance per unit area of the oxide capacitor and the SAM capacitor connected in series ($C_{diel} = (1/C_{ox} + 1/C_{SAM})^{-1}$). Thus, for large oxide thicknesses, when $C_{diel} \ll C_{SAM}$, V_{th} can be drastically larger than V_{SAM}. The term φ is introduced here to account for any contribution to the threshold voltage arising from parameters not related to the gate dielectric, such as the difference in work function between the gate electrode and the semiconductor.[27] In organic TFTs, φ is usually much smaller than the first term in eq 2, and therefore, it is often ignored. Any additional contribution from residual carriers or trapped charges are also assumed to be negligible in eq 2.[25]

A conceptually different interpretation was proposed by Possanner et al., who argued that two different physical effects of the SAMs must be taken into account. According to this interpretation, the effect of a SAM composed of dipolar molecules is a shift of the threshold voltage (approximately) equal to the absolute value of the electrostatic potential of the SAM, but opposite in sign, a situation equivalent to achieving flat-band condition:[28]

$$V_{th} = -V_{SAM} \quad (3)$$

This view, which is shared by Chung et al.,[29] cannot account for the fact that the threshold voltages of TFTs based on certain SAMs can be several tens of volts,[22,23,26] while values for V_{SAM} are never greater than a few volts.[26,30] The second effect therefore discussed by Possanner et al. is the SAM-induced formation of a space-charge layer at the semiconductor-dielectric interface that is compensated by a gate-source voltage $V_{GS} = V_{th}$ with the following value:

$$V_{th} = -\frac{\sigma}{C_{diel}} \quad (4)$$

The interfacial charge density σ can originate from a chemical reaction between the SAM and either the organic semiconductor or the oxide[31−33] or from a modification of the density of states in the semiconductor,[34] and it may include a contribution from interface trap states.

The presence of a space-charge layer implies the dependence of the threshold voltage on the capacitance of the entire gate dielectric ($V_{th} \propto 1/C_{diel}$), analogous to eq 2 and in stark contrast to eq 3. But unlike eqs 2 and 3, eq 4 does not include an explicit relation with the dipolar character of the SAM. All of the above-mentioned interpretations are based on the common ground that the SAM changes the carrier density in the semiconductor and thereby the threshold voltage. The controversy pertains to the physical or chemical mechanism(s) by which the SAM produces the observed changes in carrier density and threshold voltage, and to the question why the threshold voltage is in some experiments proportional to the inverse of the gate-dielectric capacitance (eqs 2 and 4), but in others independent of it (eq 3). A common approach to investigate the effect of the SAMs on the threshold voltage is to fabricate TFTs with SAMs based on more or less dipolar molecules and analyze the dependence of the threshold voltage on the calculated molecular dipole moment or the interfacial charge density expected from the calculated dipole moment.[24−26,29,33,35] One limitation of this approach is that the actual dipole moment of a SAM may differ from the dipole moment calculated for an individual free molecule, where depolarization effects may be important. Another drawback is that more than one mechanism may be involved when SAMs having different characteristics (e.g., chain length, chemical nature of the anchor group and/or the functional group) are employed.

To ensure a reliable and comparative study, two different SAMs were chosen, namely, an alkyl- and a fluoroalkyl-phosphonic acid SAM with the same chain length. The different functional groups will lead to different dipole moments and may induce different carrier densities in the semiconductor by affecting the chemistry at the SAM/semiconductor interface, but by keeping the anchor groups and the processing conditions and thus the bonding to the gate oxide identical, the effects of the functional groups can be isolated from any secondary effects.[36] As the gate oxide, aluminum oxide (Al_2O_3) with thickness ranging from 5 to 200 nm was deposited by atomic layer deposition (ALD). ALD produces oxide films with a small defect density and a small surface roughness while providing excellent control of the oxide thickness. In addition, Al_2O_3 is an excellent template for the formation of high-quality SAMs based on alkylphosphonic acids.[37] The benchmark organic semiconductor dinaphtho[2,3-b:2′,3′-*f*]thieno[3,2-*b*]-thiophene (DNTT) was chosen for its excellent combination of large carrier mobility and long-term stability.[38,39] Kelvin probe force microscopy (KPFM) was employed to measure the electrostatic potential originating from the SAMs as well as to get insight into the electronic interaction between the SAMs and the DNTT. In addition, atomic force microscopy (AFM) was used to confirm that the threshold voltage of the TFTs is independent of the SAM-induced semiconductor morphology.

The main conclusion from our results is that the above-mentioned relations between the SAM dipole moment and the threshold voltage cannot be generally applied. Moreover, we show that the relation between the threshold voltage and the gate-dielectric capacitance depends on the chemical nature of the SAM and the semiconductor.

2. EXPERIMENTAL SECTION

All experiments were performed using heavily doped silicon substrates onto which a layer of aluminum oxide (Al_2O_3) with a thickness of 5, 10, 50, 100 or 200 nm was deposited by ALD at a substrate temperature of 250 °C. Prior to the Al_2O_3 deposition, the native silicon dioxide was removed in dilute hydrofluoric acid. For this study, two different phosphonic acids were employed: *n*-octadecylphosphonic acid (HC_{18}−PA; purchased from PCI Synthesis) and 12,12,13,13,14,14,15,15,16,16,17,17,18,18,18-pentadecylfluoro-octadecylphosphonic acid (FC_{18}−PA; kindly provided by Matthias Schlörholz).[40] A successful SAM treatment results in a hydrophobic gate-dielectric surface, which provides the additional benefit of

DOI: 10.1021/acsami.5b02747
ACS Appl. Mater. Interfaces 2015, 7, 22775−22785

preventing the adsorption of dipolar water molecules. Measurements of the water contact angle, which is a measure of the hydrophobicity of the surface, indicate that the SAM treatment with both types of SAMs results in hydrophobic surfaces (see Figure S1), and that the water contact angle is independent of the oxide thicknesses. This observation confirms that these substrates provide a good basis for comparison. In addition to the water contact angle measurements, hexadecane contact angle measurements (41° for the HC_{18}–PA SAM and 71° for the FC_{18}–PA SAM), which are in good agreement with the previously reported values in the literature,[41,42] suggest the formation of closely packed SAMs of alkyl and fluoroakyl molecules, exposing the CH_3 and the CF_3 groups respectively to the air/film interface.[42]

For most of the experiments, the Al_2O_3-coated silicon substrates were immersed into a 2-propanol solution of either the alkyl- or the fluoroalkylphosphonic acid, resulting in a uniform coverage of the Al_2O_3 surface with one particular SAM. For some of the KPFM measurements, we also prepared substrates on which both SAMs are present. To obtain patterned substrates with both SAMs, we employed a combination of microcontact printing and immersion. In the first step, a pattern of the FC_{18}–PA SAM was produced on the Al_2O_3 surface by microcontact printing using a polydimethylsiloxane (PDMS) stamp.[43−45] Those areas of the substrate not covered by the FC_{18}–PA SAM were then filled with the HC_{18}–PA SAM by immersing the substrate into a 2-propanol solution of the alkylphosphonic acid. Substrates were then rinsed with pure 2-propanol, blow-dried with nitrogen, and baked on a hot plate at a temperature of 100 °C for 10 min to stabilize the monolayers.[45]

The organic semiconductor DNTT (purchased from Sigma-Aldrich) was deposited onto the SAM at a substrate temperature of 60 °C in a vacuum of about 10^{-6} mbar. The deposition rate and the nominal film thickness were monitored using a quartz crystal microbalance. For most of the experiments, the deposition rate was set to 0.03 nm s^{-1} and the nominal film thickness was 25 nm. For some of the experiments in which the thin-film morphology of the semiconductor was investigated, a smaller deposition rate of 0.007 nm s^{-1} was chosen, and in some experiments the nominal film thickness was 2 nm in order to obtain a partial surface coverage. Fabrication of bottom-gate, top-contact (inverted staggered) thin-film transistors was completed by the deposition of gold source and drain contacts by thermal evaporation in vacuum through a shadow mask onto the surface of the organic semiconductor layer. All TFTs have a channel length of 100 μm and a channel width of 200 μm. The gate dielectric is a combination of Al_2O_3 (deposited by ALD and having a thickness of 5, 10, 50, 100, or 200 nm) and either of the two SAMs (prepared by immersion into a 2-propanol of either the alkyl- or the fluoroalkylphosphonic acid). KPFM measurements were carried out in ambient air at room temperature using an Asylum Research Cypher equipped with conductive Ti/Ir-coated probe tips having a force constant of 1.7 N m^{-1}. Contact-mode AFM images were obtained using a Nanoscope III Multimode in ambient air using a soft cantilever (K = 0.01 N m^{-1}). AFM and KPFM images were analyzed using the WsXM software.[46]

Current–voltage measurements on the TFTs were carried out in ambient air at room temperature under yellow laboratory light, using a micromanipulator probe station and an Agilent 4156C semiconductor parameter analyzer, and using the heavily doped silicon substrate as a common gate electrode.

3. RESULTS AND DISCUSSIONS

3.1. Transistor Characteristics and Threshold Voltage. The TFTs were fabricated in the bottom-gate, top-contact architecture on silicon substrates with an Al_2O_3/SAM gate dielectric with oxide thicknesses of 5, 10, 50, 100, or 200 nm. The oxide surface was functionalized with SAMs composed of either an alkyl- or a fluoroalkylphosphonic acid, both with a chain length of 18 carbon atoms.[40] The organic semiconductor DNTT was deposited in vacuum, and the source and drain contacts were patterned using a shadow mask. The schematic cross section of the TFTs and the chemical structures of the organic semiconductor DNTT and the alkyl- and fluoroalkylphosphonic acids (HC_{18}–PA, FC_{18}–PA), are shown in Figure 1.

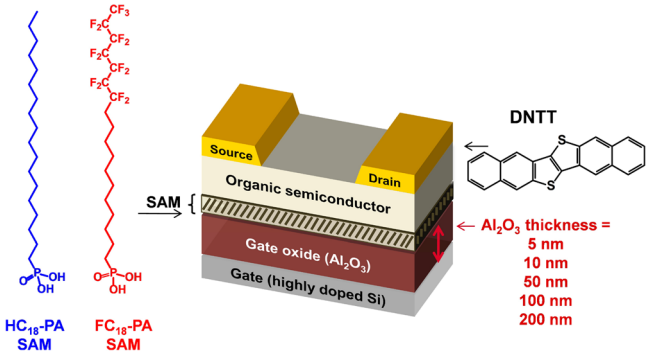

Figure 1. Schematic cross section of the TFTs, fabricated with five different Al_2O_3 thicknesses and two different phosphonic acid SAMs (HC_{18}–PA, FC_{18}–PA). Chemical structures of the organic semiconductor (DNTT) and the two phosphonic acids (HC_{18}–PA, FC_{18}–PA) are also shown.

The effect of the oxide thickness and the SAM type on the threshold voltage of the TFTs was analyzed by measuring the current–voltage characteristics of the devices. The measured transfer characteristics as well as a plot summarizing the corresponding carrier mobilities extracted from the linear regime of operation are shown in Figure 2. Regardless of the oxide thickness and the type of the SAM, all TFTs exhibit field-effect mobilities ranging from around 2 to 3.5 cm^2 V^{-1} s^{-1}, similar to the highest field-effect mobilities reported for DNTT TFTs in the literature.[38,47,48] Figure 2 also shows that independent of the oxide thickness, all TFTs in which the oxide surface was functionalized with the fluoroalkyl SAM have a more positive threshold voltage than the TFTs in which the oxide surface was functionalized with the alkyl SAM, which is consistent with previous reports.[6,22,23,40,49]

To obtain the threshold voltages of the TFTs, the measured transfer curves were fitted to the basic field-effect transistor equation:

$$I_D = \frac{\mu \cdot C_{diel} W}{L}\left[(V_{GS} - V_{th})V_{DS} - \frac{1}{2}{V_{DS}}^2\right] \quad (5)$$

where μ is the field-effect mobility, W is the channel width, L is the channel length, V_{GS} is the gate-source voltage, and V_{DS} is the drain-source voltage (−0.1 V). The gate-dielectric capacitance (C_{diel}) was calculated as follows:

$$C_{diel} = \left(\frac{1}{C_{ox}} + \frac{1}{C_{SAM}}\right)^{-1} = \varepsilon_0\left(\frac{t_{ox}}{\varepsilon_{ox}} + \frac{t_{SAM}}{\varepsilon_{SAM}}\right)^{-1} \quad (6)$$

where t_{ox} is the oxide thickness, ε_{ox} is the relative permittivity of Al_2O_3 (ε_{ox} = 9),[50] t_{SAM} is the thickness of the SAM (2.1 nm)[51] and ε_{SAM} is the relative permittivity of the SAM (ε_{SAM} = 2.5 for the HC_{18}–PA SAM, ε_{SAM} = 2.2 for the FC_{18}–PA SAM).[52] For the smallest oxide thickness (5 nm), the calculations were confirmed by frequency-dependent capacitance measurements (see Figure S2). The threshold voltages obtained for each TFT are indicated in Figure 2 and summarized in Table 1.

3.2. Electrostatic Potential Measurements. In order to understand the impact of the SAM on the threshold voltage, it

DOI: 10.1021/acsami.5b02747
ACS Appl. Mater. Interfaces 2015, 7, 22775−22785

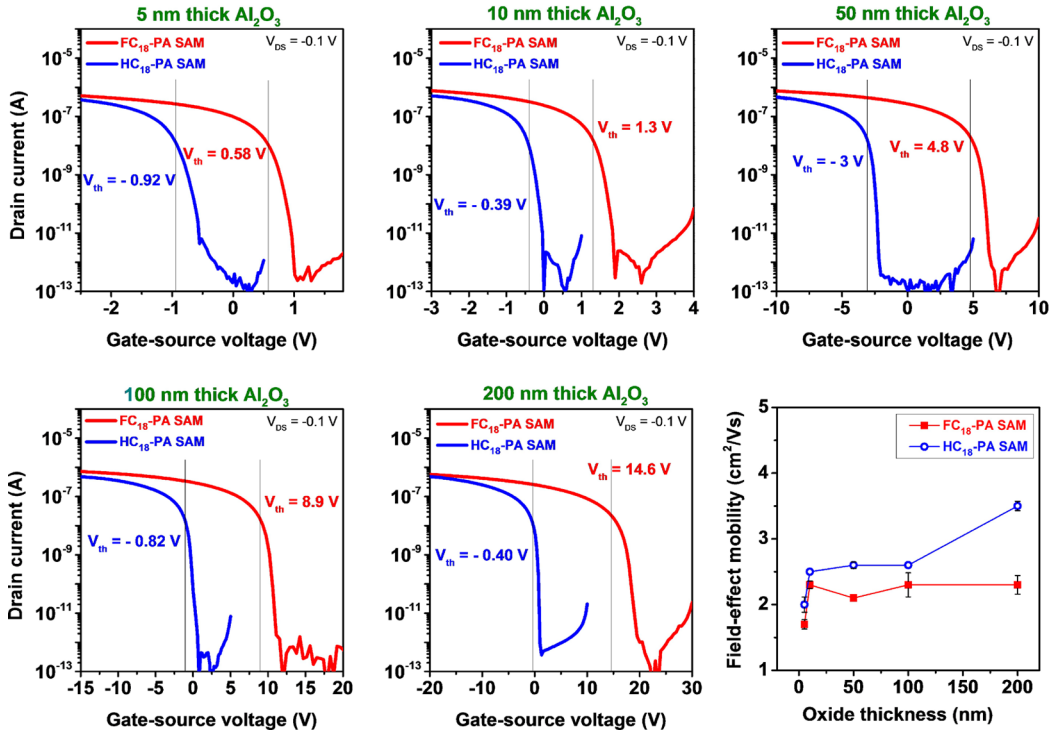

Figure 2. Measured transfer characteristics of DNTT TFTs based on five different Al_2O_3 thicknesses and two different SAMs (HC_{18}–PA, FC_{18}–PA), and field-effect mobilities extracted from the transfer characteristics of all 10 TFTs plotted as a function of the Al_2O_3 thickness (with statistical error bars). The field-effect mobilities were extracted from the linear regime (V_{DS} = −0.1 V). In each transfer curve, the threshold voltage is marked with a vertical line.

Table 1. Summary of the Gate-Dielectric Capacitances (Calculated Using eq 6) and the Threshold Voltages of DNTT TFTs (with Statistical Errors from Measuring Several TFTs) Based on Five Different Al_2O_3 Thicknesses and Two Different SAMs

	SAM capacitance [nF cm^{-2}]		threshold voltage [V]	
Al_2O_3 thickness [nm]	Al_2O_3/HC_{18}–PA	Al_2O_3/FC_{18}–PA	HC_{18}–PA SAM	FC_{18}–PA SAM
5	650[a]	580[a]	−0.92 ± 0.02	+0.58 ± 0.01
10	450	430	−0.39 ± 0.03	+1.3 ± 0.01
50	140	140	−3.0 ± 0.07	+4.8 ± 0.07
100	74	73	−0.82 ± 0.07	+8.9 ± 0.18
200	38	38	−0.40 ± 0.18	+14.6 ± 0.14

[a]For the 5 nm thick oxide, the calculations were confirmed by frequency-dependent capacitance measurements (see Figure S2).

is important to have an experimental measure of the electrostatic potential generated by the SAM (V_{SAM}). Since the actual electrostatic potential may differ from the value predicted by eq 1 due to charge rearrangements, depolarization effects (dipole–dipole interactions) and substrate-molecule interactions,[53] we employed KPFM as a noninvasive method to obtain the electrostatic potential on the surface. Since KPFM measures the contact-potential difference between the surface and the probe tip, a quantitative determination of the electrostatic potential independent of any tip effects requires using a surface reference. Moreover, the same tip must be used for comparison between different KPFM measurements. We have measured a freshly cleaved highly oriented pyrolytic graphite (HOPG) surface subsequent to each measurement as a reference to make sure the probe tip has not changed. The histograms obtained from the surface potential maps of the bare Al_2O_3 surface as well as those obtained after the functionalization with the two SAMs are shown in Figure 3. From the surface potential histograms shown in Figure 3, electrostatic potentials (relative to the Al_2O_3 surface) of +0.87 V for the

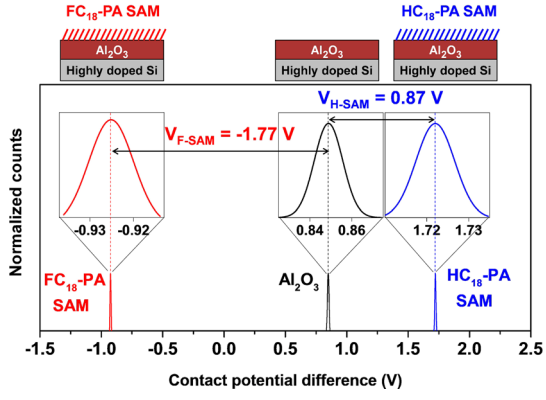

Figure 3. Surface potential histograms obtained from KPFM measurements on an Al_2O_3 surface without SAM (center), on an Al_2O_3 surface covered with the FC_{18}–PA SAM (left), and on an Al_2O_3 surface covered with the HC_{18}–PA SAM (right). The magnitude of the contact potential differences is marked with arrows between the magnified histograms shown as inset.

DOI: 10.1021/acsami.5b02747
ACS Appl. Mater. Interfaces 2015, 7, 22775–22785

Table 2. Dipole Moments of Individual HC_{18}–PA and FC_{18}–PA Molecules, and Molecular Densities, Relative Dielectric Constants, and Electrostatic Potentials of the HC_{18}–PA and FC_{18}–PA SAMs Predicted by eq 1 and Measured by KPFM[a]

SAM type	molecular dipole moment [D]	molecular density of the SAM [cm^{-2}]	relative dielectric constant	electrostatic potential predicted by eq 1 [V]	electrostatic potential measured by KPFM [V]
HC_{18}–PA	−1.07	4.55×10^{14} [ref 29] to 5.4×10^{14} [ref 54]	2.5	+0.74 to +0.88	+0.87
FC_{18}–PA	2.79	3.33×10^{14} [ref 55] to 3.7×10^{14} [ref 56]	2.2	−1.6 to − 1.77	−1.77

[a]The values for the dipole moments and relative dielectric constants are taken from Jedaa et al.,[52] and the molecular packing densities are taken from the literature either directly or were calculated for a close hexagonal packing of the molecules using the van der Waals radius of the chains.

HC_{18}–PA SAM and −1.77 V for the FC_{18}–PA SAM are obtained. Table 2 shows that the experimentally determined V_{SAM} values measured by KPFM are in good agreement with the V_{SAM} calculated using eq 1 for the densest close-packing of the chains according to the literature.

A cross-check experiment was performed using grounded gold contacts on each SAM as an in situ reference for the calibration of the work function of the probe tip (see Figure S3).

By performing the KPFM measurements on substrates with various Al_2O_3 thicknesses, we also confirmed the reasonable and commonly made assumption that the electrostatic potential of a SAM is not affected by the thickness of the oxide underneath the SAM (see Figure S4). We can therefore use the VSAM measured for an oxide thickness of 5 nm to analyze the correlation between the electrostatic potential of the SAM and the threshold voltage for all TFTs in this study, despite the different oxide thicknesses.

Comparing the measured threshold voltages (Table 1) with the measured electrostatic potentials of the SAMs (Table 2), it can be seen that the threshold voltages of the TFTs with the FC_{18}–PA SAM are significantly larger than the electrostatic potential of this SAM, at least when the oxide thickness is greater than a few tens of nanometers. For example, for an oxide thickness of 200 nm, the absolute value of the threshold voltage of the TFTs with the FC_{18}–PA SAM (∼+15 V) is almost an order of magnitude larger than the absolute value of the measured electrostatic potential of this SAM (−1.77 V). This shows that for TFTs with the fluoroalkyl SAM, eq 3 does not hold.

3.3. Relationship Between Threshold Voltage and Gate-Dielectric Capacitance. In Figure 4, the measured and predicted threshold voltages (eq 2 using the measured electrostatic potentials listed in Table 2) are plotted for different gate-dielectric capacitances. As can be seen, for both SAMs, there is a significant disagreement between the measured and the theoretically predicted values. The threshold voltages of the TFTs with the HC_{18}–PA SAM exhibit an average value of −0.64 V without any systematic dependence on the gate-dielectric capacitance, in contrast to the predicted threshold voltages from eq 2 ($V_{th} \propto 1/C_{diel}$). This value is close to the measured electrostatic potential of the HC_{18}–PA SAM, but with opposite polarity ($V_{th} \approx -V_{SAM}$), a result that is in agreement with the dipole-layer scenario proposed by Possanner et al.[28] and the experimental results from Chung et al.[29] We infer from this observation that the main effect of the oxide functionalization with the HC_{18}–PA SAM is the passivation of the charge traps at the oxide surface.[2]

Unlike the threshold voltages of the TFTs with the HC_{18}–PA SAM, which are independent of the gate-dielectric capacitance, the threshold voltages of the TFTs with the FC_{18}–PA SAM show a linear dependence on the inverse of the

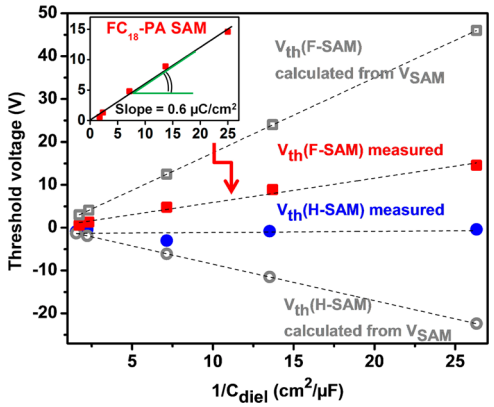

Figure 4. Measured threshold voltages (see Table 1) and threshold voltages calculated from V_{SAM} using eq 2 (using the electrostatic potentials measured by KPFM, i.e., +0.87 V for the HC_{18}–PA SAM and −1.77 V for the FC_{18}–PA SAM; see Table 2) plotted as a function of the gate-dielectric capacitance (see Table 1). For both SAMs, there is a significant disagreement between the measured and the theoretically predicted threshold voltages. The inset illustrates how the charge density σ is obtained from the slope of the linear fit using eq 4.

gate-dielectric capacitance ($V_{th} \propto 1/C_{diel}$). However, the slope of this linear relationship is only 0.6 μCcm^{-2}, which is significantly smaller than the value predicted by eq 2 (1.8 μC cm^{-2} for C_{SAM} = 1 μF cm^{-2} and V_{SAM} = −1.77 V).

Thus, for both SAMs, it is clear that eq 2 does not apply in practice, which raises the question whether there is a general relation between the dipole moment of the SAM and the threshold voltage of the TFTs, and whether this relation applies universally to all types of SAMs.

The linear relation between V_{th} and $1/C_{diel}$ for TFTs with the FC_{18}–PA SAM can be understood in terms of the space-charge layer described by eq 4. The interfacial charge density responsible for the observed $V_{th} \propto 1/C_{diel}$ dependence (see inset in Figure 4) is estimated to be $\sigma \approx -0.6$ μC cm^{-2} = -3.5×10^{12} e cm^{-2}, causing accumulation of holes in the channel, a value comparable to SAM-induced charge densities estimated experimentally for pentacene TFTs[23,57] and also to theoretical simulations.[28]

It is worth mentioning that, despite the different behavior of V_{th}, TFTs with the FC_{18}–PA SAM do not show hysteresis between the forward and backward sweeps of the transfer curves (shown in Figure S5) and exhibit a steep subthreshold swing which is compelling evidence that the interfacial charge density is not caused by shallows traps in the semiconductor.

The fact that the relationship between the gate-dielectric capacitance and the threshold voltage is so different depending on the choice of the SAM ($V_{th} \approx$ const. for the TFTs with the HC_{18}–PA SAM; $V_{th} \propto 1/C_{diel}$ for those with the FC_{18}–PA

DOI: 10.1021/acsami.5b02747
ACS Appl. Mater. Interfaces 2015, 7, 22775−22785

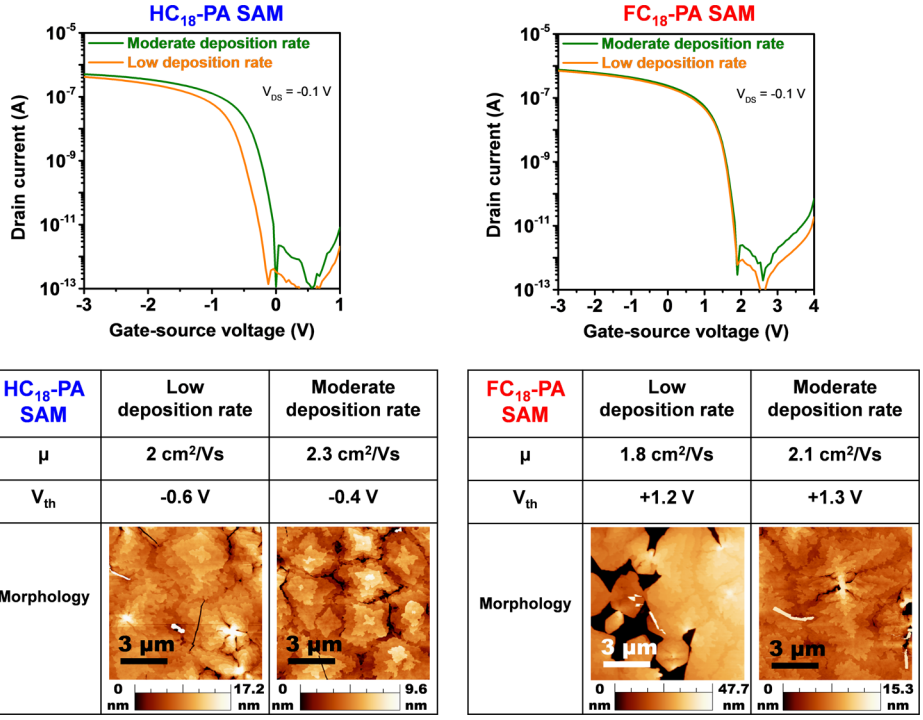

HC18-PA SAM	Low deposition rate	Moderate deposition rate
μ	2 cm²/Vs	2.3 cm²/Vs
Vth	-0.6 V	-0.4 V
Morphology	3 μm, 0 nm, 17.2 nm	3 μm, 0 nm, 9.6 nm

FC18-PA SAM	Low deposition rate	Moderate deposition rate
μ	1.8 cm²/Vs	2.1 cm²/Vs
Vth	+1.2 V	+1.3 V
Morphology	3 μm, 0 nm, 47.7 nm	3 μm, 0 nm, 15.3 nm

Figure 5. Transfer characteristics of DNTT TFTs fabricated using either of the two SAMs and with the DNTT layers deposited using either a moderate deposition rate of 0.03 nm s^{-1}or a low deposition rate of 0.007 nm s^{-1}. The Al_2O_3 gate-oxide layer has a thickness of 10 nm. The field-effect mobilities and the threshold voltages of the TFTs along with the morphology of the DNTT layers are also shown.

SAM) could be related to the presence of the strongly electronegative fluorine substituents in the FC_{18}−PA SAM. These substituents are located directly at the semiconductor/SAM interface and are likely to have a strong influence on the electronic characteristics of this interface. Before analyzing this matter, it is important to explore the possible influence of the selected SAMs on the semiconductor morphology.

3.3.1. Ruling out Semiconductor Morphology. Different SAMs can have different surface energies, which often has a significant influence on the thin-film morphology of the subsequently grown organic semiconductor layer. For many organic semiconductors, for example, pentacene, the morphology can affect the electrical TFT characteristics.[58−60] We have therefore examined the extent to which the electrical properties of our DNTT TFTs are influenced by the thin-film morphology of the DNTT layers deposited onto the two studied SAMs. In the course of these experiments, we found that the DNTT growth mode and the resulting thin-film morphology are affected not only by the choice of the SAM, but also by the DNTT deposition rate, but that these differences do not have a noticeable effect on the electrical characteristics of the TFTs.

Figure 5 shows the measured transfer characteristics of four TFTs fabricated by depositing a nominally 25 nm thick layer of DNTT onto either of the two SAMs with either a moderate or a low deposition rate (0.03 or 0.007 nm s^{-1}), along with AFM topography images of the thin-film morphology of the corresponding DNTT layers. The AFM images indicate rather pronounced differences in the DNTT morphology depending on the choice of the SAM and the deposition rate. The significant influence of the deposition rate on the thin-film morphology is also seen in much thinner DNTT layers with partial surface coverage, as shown in Figure S6. But surprisingly, these differences in the semiconductor morphology do not have a noticeable effect on the field-effect mobility or the threshold voltage of the TFTs.

Based on these observations, we rule out that the different morphology of the DNTT films on HC_{18}−PA and FC_{18}−PA functionalized substrates is responsible for the observed difference in the threshold voltage of the TFTs. Furthermore, the Al_2O_3 layer underneath the SAM is atomically smooth for all thicknesses and thus is unlikely to induce changes in the DNTT film morphology within the series of TFTs treated with the FC_{18}−PA SAM, which might cause the observed thickness-dependent V_{th} shift. In other words, neither the fact that the threshold voltages of the TFTs based on the FC_{18}−PA SAM are significantly more positive than those of the TFTs with the HC_{18}−PA SAM, nor the observation that the threshold voltage increases linearly with the inverse of the gate-dielectric capacitance in the case of the FC_{18}−PA SAM, but not in the case of the HC_{18}−PA SAM, can be explained with the different semiconductor morphologies on the two SAMs.

3.3.2. Electronic Coupling between the SAM and the Organic Semiconductor. We now turn to the question whether there are any electrostatic or electronic interactions between the SAM and the organic semiconductor that may play a role in determining the relationships between each particular SAM and the measured threshold voltages. Such possibility has been discussed in the context of charge transfer (i.e., chemical doping),[28,61,62] charge trapping,[63] and electrostatic interactions between the organic semiconductor with the local electric field of the dipolar SAM.[23,34] The latter has been proposed recently by Mityashin et al. as the mechanism responsible for the observation of a more positive threshold voltage for pentacene TFTs with fluoroalkyl-silane SAMs (in comparison to alkyl-silane SAMs) and this effect has been attributed to the accumulation of positive charge carriers due to broadening and shift of the density of states at the pentacene/SAM interface.[34]

DOI: 10.1021/acsami.5b02747
ACS Appl. Mater. Interfaces 2015, 7, 22775−22785

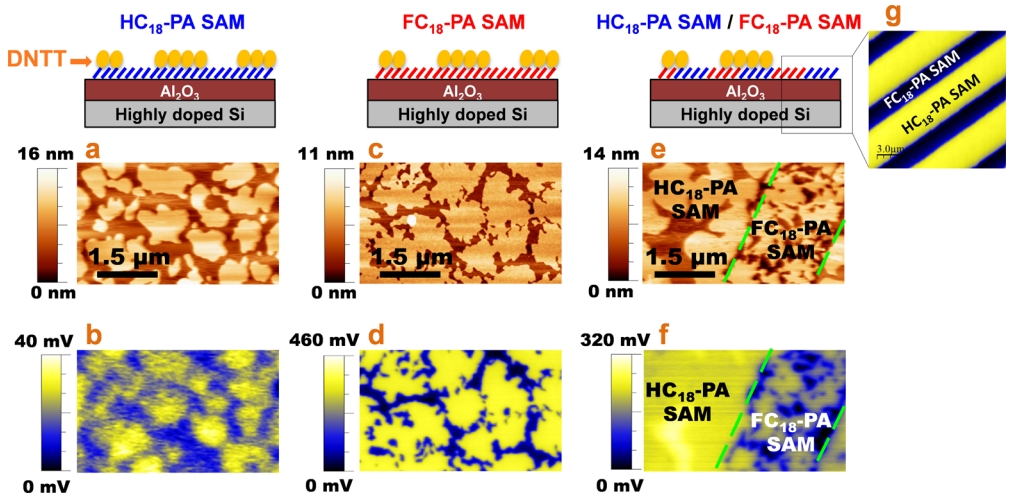

Figure 6. AFM topography images (first row) and KPFM electrostatic potential maps (second row) of a HC_{18}–PA SAM with partial DNTT coverage (a,b), of a FC_{18}–PA SAM with partial DNTT coverage (c,d), and of an array of both SAMs (produced by microcontact printing of the FC_{18}–PA SAM followed by immersion into the HC_{18}–PA molecules) with partial DNTT coverage (e,f). The contact potential difference maps have been rescaled for clarity to start from zero.

The electrostatic potential of the surface can be precisely measured by KPFM. Figure 6a–d shows AFM topography and KPFM electrostatic potential maps of a HC_{18}–PA SAM surface and of a FC_{18}–PA SAM surface, both decorated with individual, unconnected islands of DNTT (nominal DNTT thickness 2 nm).

As can be seen in Figure 6b, a small positive surface potential of about +40 mV is measured on the DNTT islands with respect to the surrounding HC_{18}–PA SAM. We presume that the positive sign is due to electronic polarization induced in the DNTT by the dipole moment of the HC_{18}–PA SAM.[64] The perpendicular components of the dipole moments of the HC_{18}–PA SAM and the FC_{18}–PA SAM point into opposite directions,[52] so if the surface potential on the DNTT located on the FC_{18}–PA SAM was also due to electronic polarization by the SAM dipole, the surface potential would be negative, that is, in the KPFM surface potential maps the DNTT islands would appear darker than the surrounding FC_{18}–PA SAM.[65] However, as Figure 6d clearly shows, a relatively large positive contact potential difference of about +0.4 V is measured between the DNTT and the FC_{18}–PA SAM, which is an order of magnitude larger than that between the DNTT and the HC_{18}–PA SAM. This suggests that there is electronic coupling between the DNTT and the FC_{18}–PA SAM that produces an interface dipole with a negative surface potential on the surface of the FC_{18}–PA SAM and a positive surface potential on the DNTT islands.

As a cross-check experiment, we also prepared a substrate on which both SAMs are present, since a patterned substrate makes it possible to measure the electrostatic potentials on the two SAMs in a single uninterrupted measurement independent of the type and the condition of the probe tip. These substrates were prepared by a combination of microcontact printing (stamping of the FC_{18}–PA SAM) and immersion (filling of the remaining areas with the HC_{18}–PA SAM). The electrostatic potential map of this patterned surface without DNTT is shown in Figure 6g. The areas with the larger (smaller) electrostatic potential correspond to the alkyl (fluoroalkyl) SAM. The measured surface-potential difference between the two SAMs prepared on the same substrate is about 0.6 V (see Figure S4), which is significantly smaller than the potential difference measured when both SAMs were prepared separately by immersion on different substrates (about 2.6 V; see Figure 3). This discrepancy is attributed to the smaller density of molecules in the microcontact-printed SAM compared to the solution-processed SAM. The potential map of the patterned surface partially covered by DNTT (Figure 6f) clearly shows a relatively large contact potential difference between the DNTT islands and the FC_{18}–PA SAM, in contrast to the small contact potential difference between the DNTT islands and the HC_{18}–PA SAM. This observation confirms the presence of a certain electronic interaction between the DNTT and the FC_{18}–PA SAM, but not between the DNTT and the HC_{18}–PA SAM. It is a priori not clear whether the interface dipole formed at the interface between the DNTT and the FC_{18}–PA SAM stems from charge transfer and/or electrostatic doping due to the electrostatic interaction between the DNTT and the FC_{18}–PA SAM. The large energy level mismatch between the highest occupied molecular orbital (HOMO) of DNTT (−5.4 eV)[47] and the lowest unoccupied molecular orbital (LUMO) of the SAM (∼ −0.2 eV for octadecyltrichlorosilane SAMs with the same chain length as our FC_{18}–PA SAM)[66] makes direct charge transfer between DNTT and the SAM unlikely.

The positive electrostatic potential on the DNTT islands on the FC_{18}–PA SAM measured by KPFM (Figure 6d) implies the accumulation of positive charges in the DNTT layer. Having already ruled out polarization and direct charge transfer, we conclude that the positive charges in the DNTT are balanced by negative charges elsewhere in the device, most likely at one of the two interfaces between the DNTT, the SAM and the Al_2O_3 layer. Although the SAM is sufficiently thin for charges to tunnel from the DNTT to the interface between the SAM and the gate oxide,[33,67] we believe that charge trapping at the SAM/Al_2O_3 interface is unlikely, since the hydroxyl groups (known to act as trap states) that are initially present on the Al_2O_3 surface are eliminated by the phosphonic acid SAM treatment. We therefore postulate that the negative charges are localized in the FC_{18}–PA SAM.

To determine whether the positive charges in the DNTT that form the space-charge layer are mobile or immobile, we will correlate the observed positive shift of the threshold voltage of the TFTs with the large positive electrostatic potential on

DOI: 10.1021/acsami.5b02747
ACS Appl. Mater. Interfaces 2015, 7, 22775–22785

the DNTT islands measured by KPFM. Assuming that the positive surface potential on the DNTT islands in Figure 6d originates from immobile positive charges in the DNTT layer, that are compensated by immobile negative charges at the FC_{18}–PA SAM/DNTT interface, a small capacitance-independent shift of the threshold voltage would be expected. Such a situation would be similar to the effect of V_{SAM} in Equation 3 and is not consistent with the observed linear dependence of V_{th} on the inverse of the dielectric capacitance. On the other hand, if there were uncompensated immobile positive charges in the semiconductor, a more negative gate-source voltage would be required to accumulate mobile holes. This would imply a negative shift of V_{th}, which is the opposite of what we obtained in our devices; see Figure 4. Having ruled out all of the above scenarios, points to the accumulation of mobile holes in the DNTT layer in close proximity to the FC_{18}–PA SAM as the most likely explanation consistent with the KPFM results and with the positive threshold voltage shifts observed in our TFTs. The accumulation of mobile holes in the DNTT layer, which is the consequence of the presence of immobile negative charges (electrons or ions) in the fluorine substituents of the SAM molecules, resembles surface chemical doping. Figure 7

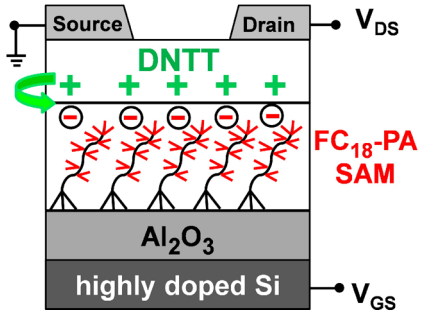

Figure 7. Schematic cross section of the DNTT TFTs with the FC_{18}–PA SAM indicating the accumulation of mobile positive charges in the DNTT layer and immobile negative charges in the SAM at the interface between DNTT and the FC_{18}–PA SAM.

illustrates that the space-charge layer, which is most probably the dominant mechanism behind the threshold voltage shifts observed in the TFTs with the FC_{18}–PA SAM, consists of mobile holes in the DNTT layer located at the interface between the DNTT and the fluorine substituents in the SAM.

A simple estimation of the charge density in the DNTT on the FC_{18}–PA SAM using a parallel plates capacitor model using $\sigma \approx C_{DNTT}V_{DNTT}$, with σ^+ and σ^- on the DNTT and the SAM surface respectively, yields a value of $\sigma \approx 2.7 \times 10^{12}$ e cm^{-2} (with $C_{DNTT} = \varepsilon_{DNTT}\varepsilon_0/d_{DNTT} \approx 0.11$ μF cm^{-2} and assuming $\varepsilon_{DNTT} = 4$ as for pentacene,[68] $d_{DNTT} = 3.2$ nm (height of a double-layered island), and $V_{DNTT} = 0.4$ V from the KPFM measurement in Figure 6d). This value, which is comparable to the previously calculated charge density from the relationship between the threshold voltage and the inverse of the gate-dielectric capacitance (Figure 4), is a result of the electronic coupling at the interface between the dielectric and the DNTT.

It is important to note that the measured surface potential stems from intrinsic electronic effects at the SAM/DNTT interface and does not include charge injection from the contacts to form the TFT channel, as is the case in a transistor. The smaller value of the charge density estimated from the surface potential compared to that obtained from the V_{th} shifts ($\sigma \approx 2.7 \times 10^{12}$ vs 3.5×10^{12} e cm^{-2}), is perhaps an indication for an additional mechanism of trapping of immobile charges at the dielectric interface upon the operation of the TFTs, as reported by Gholamrezaie et al.[63]

4. CONCLUSIONS

We have carried out a systematic investigation to unravel the mechanisms behind the shift of the threshold voltage of bottom-gate organic TFTs by the functionalization of the surface of the Al_2O_3 gate dielectric with two different SAMs. We have demonstrated that in TFTs based on a fluoroalkyl SAM, that is, a SAM with strongly electronegative fluorine substituents at the interface to the semiconductor, the threshold voltage exhibits a linear dependence on the gate-dielectric capacitance ($V_{th} \propto 1/C_{diel}$), while in TFTs based on an alkyl SAMs, the threshold voltage is independent of the dielectric capacitance and is determined mainly by the electrostatic potential generated by the SAM ($V_{th} \approx -V_{SAM}$).

To shed light on this dissimilar behavior, we have presented a detailed nanoscale investigation of the electrostatic potential of the SAM/organic semiconductor interface by means of KPFM. Our results provide evidence for an electronic coupling and the formation of a space-charge layer consisting of mobile holes at the interface between the DNTT and the fluoroalkyl SAM, which is responsible for the observed dependence of the threshold voltage on the gate-dielectric capacitance. In contrast, no evidence for such interfacial electrostatic interaction was detected for the combination of DNTT and the alkyl SAM. We thereby confirm the validity of the two vigorously debated cases ($V_{th} \propto 1/C_{diel}$ and $V_{th} \approx -V_{SAM}$) by showing that both of them are essential to explain the threshold-voltage shifts observed in organic TFTs due to SAMs at the semiconductor/dielectric interface. Our method of determining the electrostatic potential difference between the SAM and the semiconductor is thus a promising approach to select the proper combination of oxide thickness, SAM and organic semiconductor to tune the threshold voltage, which is an important aspect in the design of integrated circuits. We conclude that the mechanism by which the gate-dielectric modification with a SAM affects the threshold voltage of organic TFTs is ultimately related to the properties of the interface between the SAM and the organic semiconductor and can therefore not be ascribed solely to the dipole moment of the SAM.

■ ASSOCIATED CONTENT

Supporting Information

The Supporting Information is available free of charge on the ACS Publications website at DOI: 10.1021/acsami.5b02747.

Water contact angle measurements on Al_2O_3 with five different thicknesses (Figure S1), frequency-dependent capacitance measurements on the 5 nm thick Al_2O_3 (Figure S2), KPFM electrostatic potential measurements on the SAMs with a grounded gold contact (Figure S3), KPFM measurements on the Al_2O_3 patterned with both SAMs (Figure S4), hysteresis-free transfer curves (forward and backward sweeps) of the TFTs functionalized with the FC_{18}–PA SAM (Figure S5), and AFM topography images of DNTT partial layer morphology and further discussions on the DNTT growth (Figure S6) (PDF)

DOI: 10.1021/acsami.5b02747
ACS Appl. Mater. Interfaces 2015, 7, 22775–22785

AUTHOR INFORMATION

Corresponding Authors

*E-mail: Ebarrena@icmab.es.
*E-mail: H.Klauk@fkf.mpg.de.

Notes

The authors declare no competing financial interest.

ACKNOWLEDGMENTS

This work was partially funded by the German Ministry of Education and Research (BMBF) under Grant 1612000463 (KoSiF) and by the Spanish MINECO project MAT2013-47869-C4-1-P. We also acknowledge financial aid from the Generalitat de Catalunya (2014 SGR 501). M.A. would like to thank Marion Hagel at the Max Planck Institute for Solid State Research for expert technical assistance, and Ulrike Kraft at the Max Planck Institute for Solid State Research for assistance with the capacitance measurements. The authors also acknowledge David Gundlach at the National Institute for Standards and Technology for fruitful discussions.

REFERENCES

(1) Lin, Y.-Y.; Gundlach, D. J.; Nelson, S. F.; Jackson, T. N. Stacked Pentacene Layer Organic Thin-Film Transistors with Improved Characteristics. *IEEE Electron Device Lett.* **1997**, *18*, 606−608.

(2) Chua, L.-L.; Zaumseil, J.; Chang, J.-F.; Ou, E. C.-W.; Ho, P. K.-H.; Sirringhaus, H.; Friend, R. H. General Observation of N-type Field-effect Behaviour in Organic Semiconductors. *Nature* **2005**, *434*, 194−199.

(3) Hutchins, D. O.; Weidner, T.; Baio, J.; Polishak, B.; Acton, O.; Cernetic, N.; Ma, H.; Jen, A. K.-Y. Morphology and Thin Film Transistor Device Performance. *J. Mater. Chem. C* **2013**, *1*, 101−113.

(4) Lin, Y.-Y.; Gundlach, D. J.; Nelson, S. F.; Jackson, T. N. Pentacene-Based Organic Thin-film Transistors. *IEEE Trans. Electron Devices* **1997**, *44*, 1325−1331.

(5) Gundlach, D. J.; Kuo, C.-C. S.; Sheraw, C. D.; Nichols, J. A.; Jackson, T. N. Improved Organic Thin Film Transistor Performance Using Chemically-Modified Gate Dielectrics. *Proc. SPIE* **2001**, *4466*, 54−64.

(6) Martinez-Hardigree, J. F.; Dawidczyk, T. J.; Ireland, R. M.; Johns, G. L.; Jung, B.; Nyman, M.; Osterbacka, R.; Markovic, N.; Katz, H. E. Reducing Leakage Currents in n-Channel Organic Field-Effect Transistors Using Molecular Dipole Monolayers on Nanoscale Oxides. *ACS Appl. Mater. Interfaces* **2013**, *5*, 7025−7032.

(7) Hofmockel, R.; Zschieschang, U.; Kraft, U.; Rödel, R.; Hansen, N. H.; Stolte, M.; Würthner, F.; Takimiya, K.; Kern, K.; Pflaum, J.; Klauk, H. High-mobility Organic Thin-film Transistors Based on a Small-molecule Semiconductor Deposited in Vacuum and by Solution Shearing. *Org. Electron.* **2013**, *14*, 3213−3221.

(8) Kelley, T. W.; Boardman, L. D.; Dunbar, T. D.; Muyres, D. V.; Pellerite, M. J.; Smith, T. P. High-Performance OTFTs Using Surface-Modified Alumina Dielectrics. *J. Phys. Chem. B* **2003**, *107*, 5877−5881.

(9) Yoon, W.-J.; Berger, P. R. Atomic Layer Deposited HfO2 Gate Dielectrics for Low-voltage Operating, High-performance Poly-(3-hexythiophene) Organic Thin-film Transistors. *Org. Electron.* **2010**, *11*, 1719−1722.

(10) Acton, O.; Ting, G. G.; Shamberger, P. J.; Ohuchi, F. S.; Ma, H.; Jen, A. K.-Y. Dielectric Surface-controlled Low-voltage Organic Transistors via N-alkyl Phosphonic Acid Self-assembled Monolayers on High-k Metal Oxide. *ACS Appl. Mater. Interfaces* **2010**, *2*, 511−520.

(11) Acton, O.; Dubey, M.; Weidner, T.; O'Malley, K. M.; Kim, T.-W.; Ting, G. G.; Hutchins, D.; Baio, J. E.; Lovejoy, T. C.; Gage, A. H.; et al. Simultaneous Modification of Bottom-Contact Electrode and Dielectric Surfaces for Organic Thin-Film Transistors Through Single-Component Spin-Cast Monolayers. *Adv. Funct. Mater.* **2011**, *21*, 1476−1488.

(12) Cernetic, N.; Acton, O.; Weidner, T.; Hutchins, D. O.; Baio, J. E.; Ma, H.; Jen, A. K.-Y. Bottom-contact Small-molecule N-type Organic Field Effect Transistors Achieved via Simultaneous Modification of Electrode and Dielectric Surfaces. *Org. Electron.* **2012**, *13*, 3226−3233.

(13) Wei, Q.; You, E.; Hendricks, N. R.; Briseno, A. L.; Watkins, J. J. Flexible Low-voltage Polymer Thin-film Transistors Using Supercritical CO_2-deposited ZrO_2 Dielectrics. *ACS Appl. Mater. Interfaces* **2012**, *4*, 2322−2324.

(14) Park, Y. M.; Desai, A.; Salleo, A.; Jimison, L. Solution-Processable Zirconium Oxide Gate Dielectrics for Flexible Organic Field Effect Transistors Operated at Low Voltages. *Chem. Mater.* **2013**, *25*, 2571−2579.

(15) Beaulieu, M. R.; Baral, J. K.; Hendricks, N. R.; Tang, Y.; Briseño, A. L.; Watkins, J. J. Solution Processable High Dielectric Constant Nanocomposites Based on ZrO2 Nanoparticles for Flexible Organic Transistors. *ACS Appl. Mater. Interfaces* **2013**, *5*, 13096−13103.

(16) Xia, G.; Wang, S.; Zhao, X.; Zhou, L. High-performance Low-voltage Organic Transistor Memories with Room-temperature Solution-processed Hybrid Nanolayer Dielectrics. *J. Mater. Chem. C* **2013**, *1*, 3291.

(17) Lee, W.-H.; Wang, C.-C.; Chen, W.-T.; Ho, J.-C. Characteristic of Organic Thin Film Transistor with a High- k Insulator of Nano-TiO 2 and Polyimide Blend. *Jpn. J. Appl. Phys.* **2008**, *47*, 8955−8960.

(18) Tang, M. L.; Okamoto, T.; Bao, Z. High-Performance Organic Semiconductors: Asymmetric Linear Acenes Containing Sulphur. *J. Am. Chem. Soc.* **2006**, *128*, 16002−16003.

(19) Bram, C.; Jung, C.; Stratmann, M. Self Assembled Molecular Monolayers on Oxidized Inhomogeneous Aluminum Surfaces. *Fresenius' J. Anal. Chem.* **1997**, *358*, 108−111.

(20) Ma, H.; Acton, O.; Hutchins, D. O.; Cernetic, N.; Jen, A. K.-Y. Multifunctional Phosphonic Acid Self-assembled Monolayers on Metal Oxides as Dielectrics, Interface Modification Layers and Semiconductors for Low-voltage High-performance Organic Field-effect Transistors. *Phys. Chem. Chem. Phys.* **2012**, *14*, 14110−14126.

(21) Halik, M.; Hirsch, A. The Potential of Molecular Self-Assembled Monolayers in Organic Electronic Devices. *Adv. Mater.* **2011**, *23*, 2689−2695.

(22) Kobayashi, S.; Nishikawa, T.; Takenobu, T.; Mori, S.; Shimoda, T.; Mitani, T.; Shimotani, H.; Yoshimoto, N.; Ogawa, S.; Iwasa, Y. Control of Carrier Density by Self-assembled Monolayers in Organic Field-effect Transistors. *Nat. Mater.* **2004**, *3*, 317−322.

(23) Pernstich, K. P.; Haas, S.; Oberhoff, D.; Goldmann, C.; Gundlach, D. J.; Batlogg, B.; Rashid, A. N.; Schitter, G. Threshold Voltage Shift in Organic Field Effect Transistors by Dipole Monolayers on the Gate Insulator. *J. Appl. Phys.* **2004**, *96*, 6431.

(24) Huang, C.; Katz, H. E.; West, J. E. Solution-Processed Organic Field-Effect Transistors and Unipolar Inverters Using Self-Assembled Interface Dipoles on Gate Dielectrics. *Langmuir* **2007**, *23*, 13223−13231.

(25) Salinas, M.; Jäger, C. M.; Amin, A. Y.; Dral, P. O.; Meyer-Friedrichsen, T.; Hirsch, A.; Clark, T.; Halik, M. The Relationship Between Threshold Voltage and Dipolar Character of Self-assembled Monolayers in Organic Thin-film Transistors. *J. Am. Chem. Soc.* **2012**, *134*, 12648−12652.

(26) Celle, C.; Suspène, C.; Ternisien, M.; Lenfant, S.; Guérin, D.; Smaali, K.; Lmimouni, K.; Simonato, J. P.; Vuillaume, D. Interface Dipole: Effects on Threshold Voltage and Mobility for Both Amorphous and Poly-crystalline Organic Field Effect Transistors. *Org. Electron.* **2014**, *15*, 729−737.

(27) Nausieda, I.; Ryu, K. K.; He, D. D.; Akinwande, A. I.; Bulovic, V.; Sodini, C. G. Dual Threshold Voltage Organic Thin-Film Transistor Technology. *IEEE Trans. Electron Devices* **2010**, *57*, 3027−3032.

(28) Possanner, S. K.; Zojer, K.; Pacher, P.; Zojer, E.; Schürrer, F. Threshold Voltage Shifts in Organic Thin-Film Transistors Due to Self-Assembled Monolayers at the Dielectric Surface. *Adv. Funct. Mater.* **2009**, *19*, 958−967.

DOI: 10.1021/acsami.5b02747
ACS Appl. Mater. Interfaces 2015, 7, 22775−22785

(29) Chung, Y.; Verploegen, E.; Vailionis, A.; Sun, Y.; Nishi, Y.; Murmann, B.; Bao, Z. Controlling Electric Dipoles in Nanodielectrics and Its Applications for Enabling Air-stable N-channel Organic Transistors. *Nano Lett.* **2011**, *11*, 1161−1165.
(30) Sugimura, H.; Hayashi, K.; Saito, N.; Nakagiri, N.; Takai, O. Surface Potential Microscopy for Organized Molecular Systems. *Appl. Surf. Sci.* **2002**, *188*, 403−410.
(31) Pacher, P.; Lex, A.; Proschek, V.; Etschmaier, H.; Tchernychova, E.; Sezen, M.; Scherf, U.; Grogger, W.; Trimmel, G.; Slugovc, C.; Zojer, E. Chemical Control of Local Doping in Organic Thin-Film Transistors: From Depletion to Enhancement. *Adv. Mater.* **2008**, *20*, 3143−3148.
(32) Ausserlechner, S. J.; Gruber, M.; Hetzel, R.; Flesch, H.-G.; Ladinig, L.; Hauser, L.; Haase, A.; Buchner, M.; Resel, R.; Schürrer; Stadlober, B.; Trimmel, G.; Zojer, K.; Zojer, E. Mechanism of Surface Proton Transfer Doping in Pentacene Based Organic Thin-film Transistors. *Phys. Status Solidi A* **2012**, *209*, 181−192.
(33) Fleischli, F. D.; Suárez, S.; Schaer, M.; Zuppiroli, L. Organic Thin-film Transistors: The Passivation of the Dielectric-pentacene Interface by Dipolar Self-assembled Monolayers. *Langmuir* **2010**, *26*, 15044−15049.
(34) Mityashin, A.; Roscioni, O. M.; Muccioli, L.; Zannoni, C.; Geskin, V.; Janssen, D.; Steudel, S.; Genoe, J.; Heremans, P. Multiscale Modeling of the Electrostatic Impact of Self-Assembled Monolayers Used as Gate Dielectric Treatment in Organic Thin-Film Transistors. *ACS Appl. Mater. Interfaces* **2014**, *6*, 15372−15378.
(35) Celle, C.; Suspène, C.; Simonato, J.-P.; Lenfant, S.; Ternisien, M.; Vuillaume, D. Self-assembled Monolayers for Electrode Fabrication and Efficient Threshold Voltage Control of Organic Transistors with Amorphous Semiconductor Layer. *Org. Electron.* **2009**, *10*, 119−126.
(36) Devices without SAM were not investigated in this study, since oxide surfaces without SAM passivation are characterized by a significant density of hydroxyl groups and hence a significant density of charge traps. They are also hydrophilic and thus usually covered with a thin layer of water and airborne contaminants. As a result, their characteristics are ill-defined and thus they are not a good basis for comparison.
(37) Folkers, J. P.; Gorman, C. B.; Laibinis, P. E.; Buchholz, S.; Whitesides, G. M.; Nuzzo, R. G. Self-Assembled Monolayers of Long-chain Hydroxamic Acids on the Native Oxides of Metals1. *Langmuir* **1995**, *11*, 813−824.
(38) Zschieschang, U.; Ante, F.; Kälblein, D.; Yamamoto, T.; Takimiya, K.; Kuwabara, H.; Ikeda, M.; Sekitani, T.; Someya, T.; Blochwitz-Nimoth, J.; Klauk, H. Dinaphtho[2,3-b:2′,3′-f]thieno[3,2-b]thiophene (DNTT) Thin-film Transistors with Improved Performance and Stability. *Org. Electron.* **2011**, *12*, 1370−1375.
(39) Głowacki, E. D.; Irimia-Vladu, M.; Kaltenbrunner, M.; Gsiorowski, J.; White, M. S.; Monkowius, U.; Romanazzi, G.; Suranna, G. P.; Mastrorilli, P.; Sekitani, T.; Bauer, S.; Someya, T.; Torsi, L.; Sariciftci, N. S. Hydrogen-bonded Semiconducting Pigments for Air-stable Field-effect Transistors. *Adv. Mater.* **2013**, *25*, 1563−1569.
(40) Zschieschang, U.; Ante, F.; Schlörholz, M.; Schmidt, M.; Kern, K.; Klauk, H. Mixed Self-assembled Monolayer Gate Dielectrics for Continuous Threshold Voltage Control in Organic Transistors and Circuits. *Adv. Mater.* **2010**, *22*, 4489−4493.
(41) Pellerite, M. J.; Dunbar, T. D.; Boardman, L. D.; Wood, E. J. Effects of Fluorination on Self-Assembled Monolayer Formation from Alkanephosphonic Acids on Aluminum: Kinetics and Structure. *J. Phys. Chem. B* **2003**, *107*, 11726−11736.
(42) Brukman, M. J.; Marco, G. O.; Dunbar, T. D.; Boardman, L. D.; Carpick, R. W. Nanotribological Properties of Alkanephosphonic Acid Self-Assembled Monolayers on Aluminum Oxide: Effects of Fluorination and Substrate Crystallinity. *Langmuir* **2006**, *22*, 3988−3998.
(43) Zschieschang, U.; Halik, M.; Klauk, H. Microcontact-Printed Self-Assembled Monolayers as Ultrathin Gate Dielectrics in Organic Thin-Film Transistors and Complementary Circuits. *Langmuir* **2008**, *24*, 1665−1669.
(44) Hirata, I.; Zschieschang, U.; Ante, F.; Yokota, T.; Kuribara, K.; Yamamoto, T.; Takimiya, K.; Ikeda, M.; Kuwabara, H.; Klauk, H.; Sekitani, T.; Someya, T. Spatial Control of the Threshold Voltage of Low-voltage Organic Transistors by Microcontact Printing of Alkyl- and Fluoroalkyl-phosphonic Acids. *MRS Commun.* **2011**, *1*, 33−36.
(45) Goetting, L. B.; Deng, T.; Whitesides, G. M. Microcontact Printing of Alkanephosphonic Acids on Aluminum: Pattern Transfer by Wet Chemical Etching. *Langmuir* **1999**, *15*, 1182−1191.
(46) Horcas, I.; Fernández, R.; Gómez-Rodríguez, J. M.; Colchero, J.; Gómez-Herrero, J.; Baro, A. M. WSXM: a Software for Scanning Probe Microscopy and a Tool for Nanotechnology. *Rev. Sci. Instrum.* **2007**, *78*, 013705.
(47) Yamamoto, T.; Takimiya, K. Facile Synthesis of Highly π-Extended Heteroarenes, Application to Field-Effect Transistors. *J. Am. Chem. Soc.* **2007**, *129*, 2224−2225.
(48) Kaltenbrunner, M.; Sekitani, T.; Reeder, J.; Yokota, T.; Kuribara, K.; Tokuhara, T.; Drack, M.; Schwödiauer, R.; Graz, I.; Bauer-Gogonea, S.; Bauer, S.; Someya, T. An Ultra-lightweight Design for Imperceptible Plastic Electronics. *Nature* **2013**, *499*, 458−463.
(49) Kraft, U.; Zschieschang, U.; Ante, F.; Kälblein, D.; Kamella, C.; Amsharov, K.; Jansen, M.; Kern, K.; Weber, E.; Klauk, H. Fluoroalkylphosphonic Acid Self-assembled Monolayer Gate Dielectrics for Threshold-voltage Control in Low-voltage Organic Thin-film Transistors. *J. Mater. Chem.* **2010**, *20*, 6416.
(50) Robertson, J. High Dielectric Constant Oxides. *Eur. Phys. J.: Appl. Phys.* **2004**, *28*, 265−291.
(51) Klauk, H.; Zschieschang, U.; Pflaum, J.; Halik, M. Ultralow-power Organic Complementary Circuits. *Nature* **2007**, *445*, 745−748.
(52) Jedaa, A.; Salinas, M.; Jäger, C. M.; Clark, T.; Ebel, A.; Hirsch, A.; Halik, M. Mixed Self-assembled Monolayer of Molecules with Dipolar and Acceptor character—Influence on Hysteresis and Threshold Voltage in Organic Thin-film Transistors. *Appl. Phys. Lett.* **2012**, *100*, 063302.
(53) Heimel, G.; Rissner, F.; Zojer, E. Modeling the Electronic Properties of Pi-conjugated Self-assembled Monolayers. *Adv. Mater.* **2010**, *22*, 2494−2513.
(54) Hanson, E. L.; Schwartz, J.; Nickel, B.; Koch, N.; Danisman, M. F. Bonding Self-Assembled, Compact Organophosphonate Monolayers to the Native Oxide Surface of Silicon. *J. Am. Chem. Soc.* **2003**, *125*, 16074−16080.
(55) Barriet, D.; Lee, T. R. Fluorinated Self-assembled Monolayers: Composition, Structure and Interfacial Properties. *Curr. Opin. Colloid Interface Sci.* **2003**, *8*, 236−242.
(56) Ciferri, A. *Supramolecular Polymers*; Marcel Dekker, Inc.: New York, Basel, 2000; Chapter 10, p 443.
(57) Von Mühlenen, A.; Castellani, M.; Schaer, M.; Zuppiroli, L. Controlling Charge-transfer at the Gate Interface of Organic Field-effect Transistors. *Phys. Status Solidi B* **2008**, *245*, 1170−1174.
(58) Yang, S. Y.; Shin, K.; Park, C. E. The Effect of Gate-Dielectric Surface Energy on Pentacene Morphology and Organic Field-Effect Transistor Characteristics. *Adv. Funct. Mater.* **2005**, *15*, 1806−1814.
(59) Di Carlo, A.; Piacenza, F.; Bolognesi, A.; Stadlober, B.; Maresch, H. Influence of Grain Sizes on the Mobility of Organic Thin-film Transistors. *Appl. Phys. Lett.* **2005**, *86*, 263501.
(60) Miyadera, T.; Wang, S. D.; Minari, T.; Tsukagoshi, K.; Aoyagi, Y. Charge Trapping Induced Current Instability in Pentacene Thin Film Transistors: Trapping Barrier and Effect of Surface Treatment. *Appl. Phys. Lett.* **2008**, *93*, 033304.
(61) Suemori, K.; Uemura, S.; Yoshida, M.; Hoshino, S.; Takada, N.; Kodzasa, T.; Kamata, T. Threshold Voltage Stability of Organic Field-effect Transistors for Various Chemical Species in the Insulator Surface. *Appl. Phys. Lett.* **2007**, *91*, 192112.
(62) Ellison, D. J.; Lee, B.; Podzorov, V.; Frisbie, C. D. Surface Potential Mapping of SAM-functionalized Organic Semiconductors by Kelvin Probe Force Microscopy. *Adv. Mater.* **2011**, *23*, 502−507.
(63) Gholamrezaie, F.; Andringa, A.-M.; Roelofs, W. S. C.; Neuhold, A.; Kemerink, M.; Blom, P. W. M.; de Leeuw, D. M. Charge Trapping

DOI: 10.1021/acsami.5b02747
ACS Appl. Mater. Interfaces 2015, 7, 22775−22785

by Self-assembled Monolayers as the Origin of the Threshold Voltage Shift in Organic Field-effect Transistors. *Small* **2012**, *8*, 241−245.
(64) Wu, Y.; Haugstad, G.; Frisbie, C. D. Electronic Polarization at Pentacene/Polymer Dielectric Interfaces: Imaging Surface Potentials and Contact Potential Differences as a Function of Substrate Type, Growth Temperature, and Pentacene Microstructure. *J. Phys. Chem. C* **2014**, *118*, 2487−2497.
(65) In the electrostatic model of a perfectly ordered array of dipoles and for vertical length scales larger than the intermolecular distance of the molecules in the SAM (∼0.5 nm), there is no electric field outside the SAM. However, this assumption fails for immediate proximity, implying that an organic molecule in contact with the SAM may feel a local electric field at the interface. For more detail, consult: Natan, A.; Kronik, L.; Haick, H.; Tung, R. T. Electrostatic Properties of Ideal and Non-ideal Polar Organic Monolayers: Implications for Electronic Devices. *Adv. Mater.* **2007**, *19*, 4103−4117.
(66) Boulas, C.; Davidovits, J. V.; Rondelez, F.; Vuillaume, D. Suppression of Charge Carrier Tunneling Through Organic Self-Assembled Monolayers. *Phys. Rev. Lett.* **1996**, *76*, 4797−4800.
(67) Suárez, S.; Fleischli, F. D.; Schaer, M.; Zuppiroli, L. From Oxide Surface to Organic Transistor Properties: The Nature and the Role of Oxide Gate Surface Defects. *J. Phys. Chem. C* **2010**, *114*, 7153−7160.
(68) Lee, J.; Hwang, D. K.; Park, C. H.; Kim, S. S.; Im, S. Pentacene-based Photodiode with Schottky Junction. *Thin Solid Films* **2004**, *451−452*, 12−15.

DOI: 10.1021/acsami.5b02747
ACS Appl. Mater. Interfaces 2015, 7, 22775−22785

Supporting Information for

Threshold-Voltage Shifts in Organic Transistors Due to Self-Assembled Monolayers at the Dielectric: Evidence for Electronic Coupling and Dipolar Effects

*Mahdieh Aghamohammadi,[1] Reinhold Rödel,[1] Ute Zschieschang,[1] Carmen Ocal,[2] Hans Boschker,[1] R. Thomas Weitz,[3,4] Esther Barrena, *[2] and Hagen Klauk *[1]*

1 Max Planck Institute for Solid State Research, Heisenbergstr. 1, 70569, Stuttgart, Germany

2 Instituto de Ciencia de Materiales de Barcelona (ICMAB-CSIC), Campus de la UAB, 08193 Bellaterra, Spain

3 BASF SE, GMV/T – J542s, 67056 Ludwigshafen, Germany

4 Innovation Lab GmbH, Speyerer Str. 4, 69115 Heidelberg, Germany

Corresponding Author

* Email: Ebarrena@icmab.es

* Email: H.Klauk@fkf.mpg.de

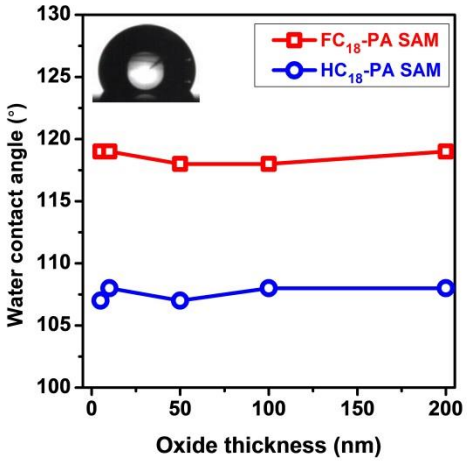

Al_2O_3 thickness	Water contact angle obtained from HC_{18}-PA SAM	Water contact angle obtained from FC_{18}-PA SAM
5 nm	107 °	119 °
10 nm	108 °	119 °
50 nm	107 °	118 °
100 nm	108 °	118 °
200 nm	108 °	119 °

Figure S1. Water contact angles measured on silicon substrates coated with a 5 nm, 10 nm, 50 nm, 100 nm or 200 nm thick layer of Al_2O_3 (deposited by atomic layer deposition) and functionalized with either the HC_{18}-PA or the FC_{18}-PA SAM. The large contact angles compared to an untreated Al_2O_3 surface (less than 20°) confirm the formation of closely-packed SAMs.

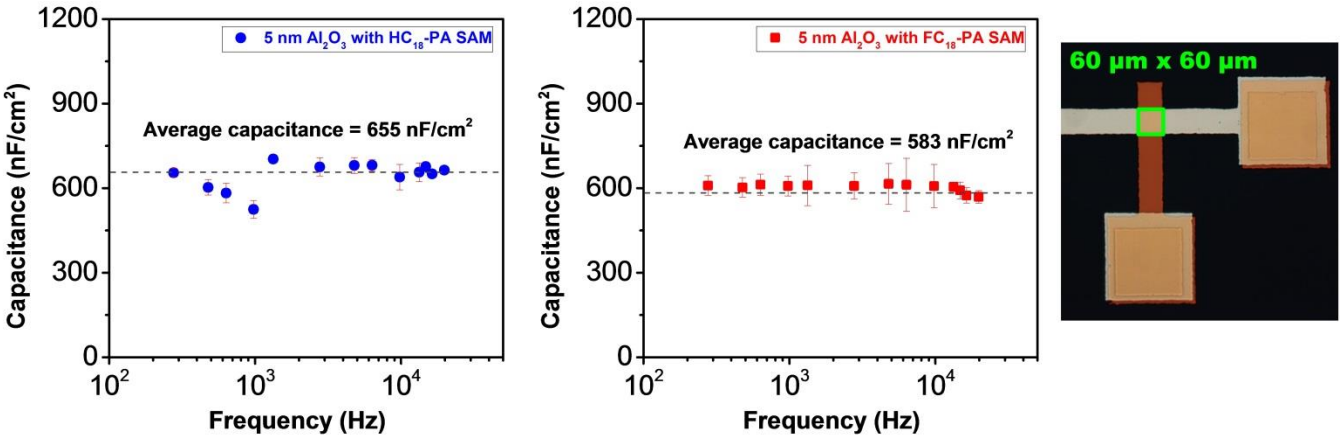

Figure S2. Frequency-dependent capacitances measured on Al/ Al_2O_3/ SAM/ Au capacitors to confirm the capacitances calculated using Equation 6. The Al_2O_3 layer has a thickness of 5 nm and was functionalized with either the HC_{18}-PA SAM (left) or the FC_{18}-PA SAM (right). The capacitors have an area of 60 µm × 60 µm.

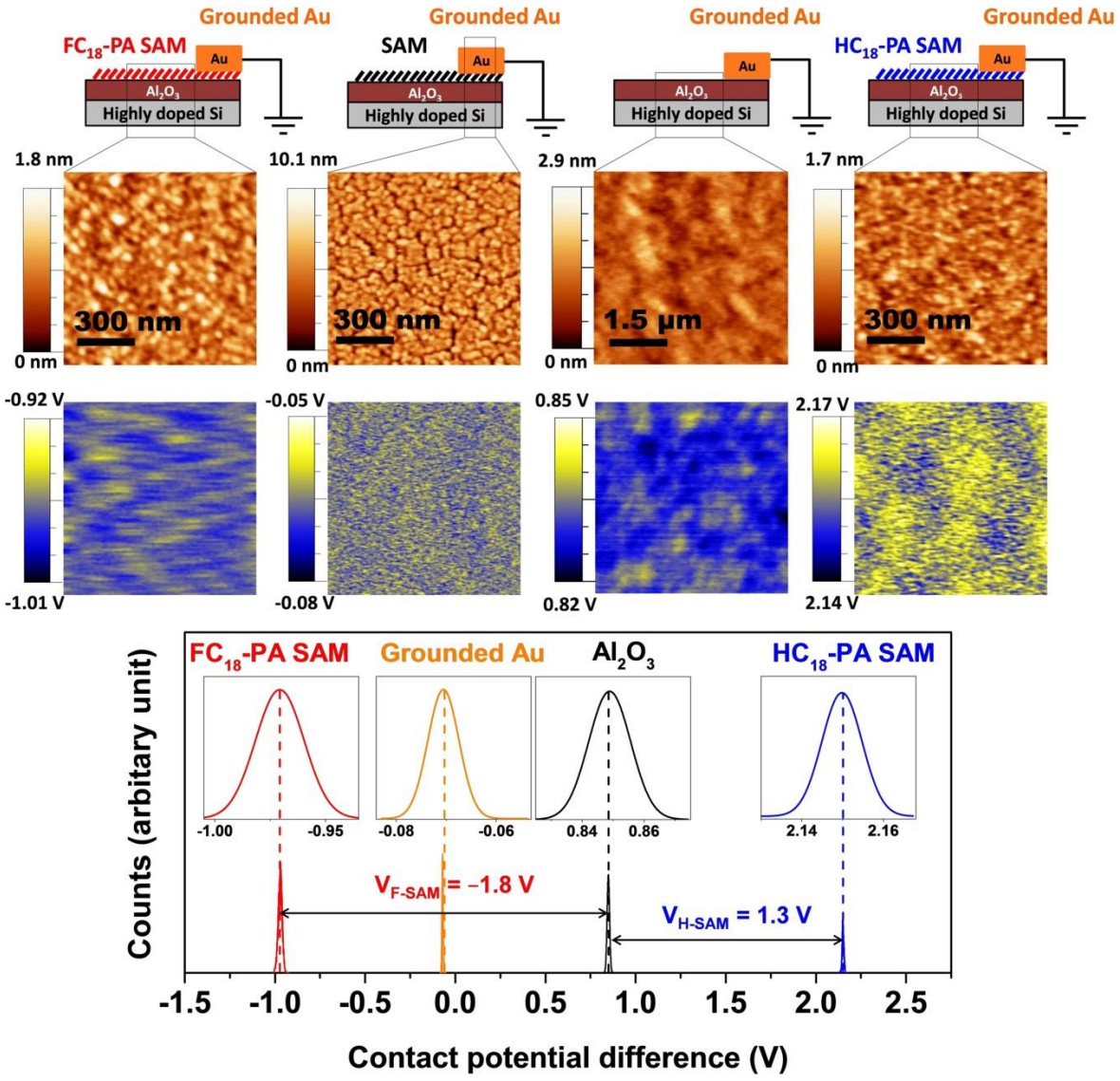

Figure S3. Estimation of the electrostatic potential of the SAMs. In these measurements, a gold electrode, deposited onto each substrate and connected to ground potential, served as an in-situ reference for the work function of the probe tip. Top: AFM topography images (first row) and KPFM electrostatic potential maps (second row) of an Al_2O_3 surface covered with the FC_{18}-PA SAM, of an Al_2O_3 surface covered with the HC_{18}-PA SAM, of an Al_2O_3 surface without SAM and of the grounded Au electrode. Bottom: contact potential differences obtained from the surface potential histograms, with values slightly larger in magnitude than those obtained from the measurements in which HOPG served as a reference (see in Figure 3). The values measured relative to the HOPG reference (Figure 3) are believed to be more reliable, since the deposited gold contact may affect the local electronic properties of the SAM underneath.

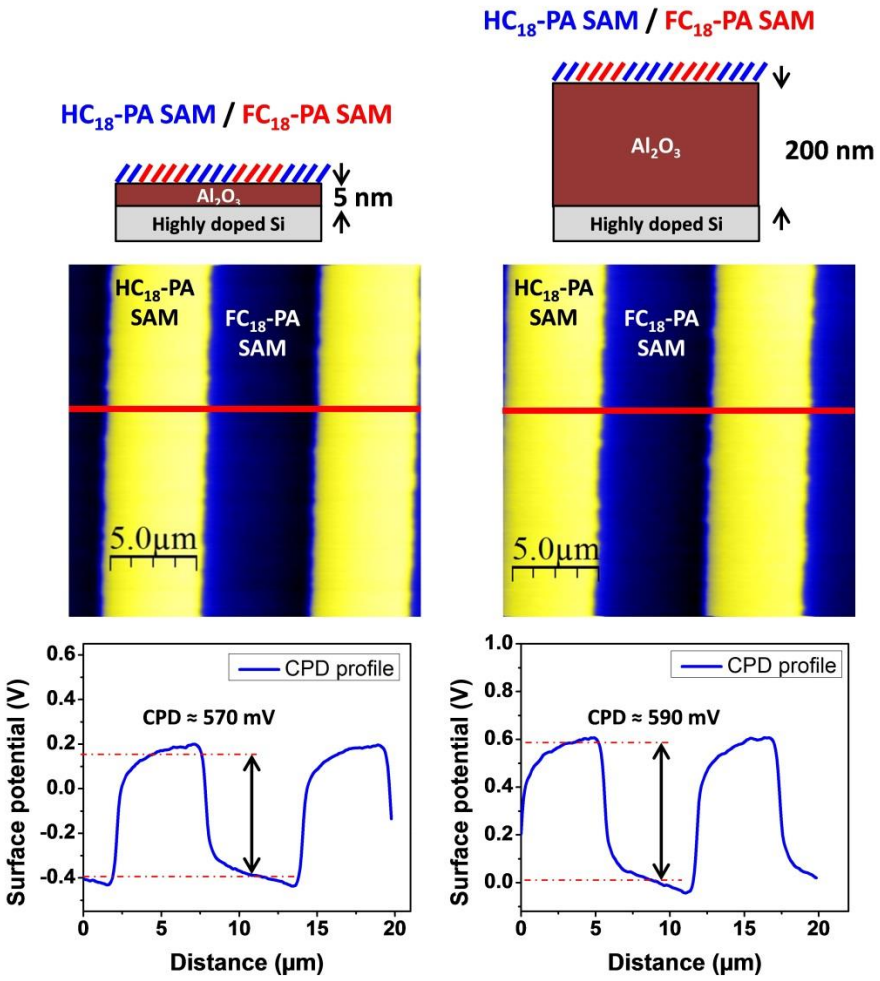

Figure S4. KPFM electrostatic potential maps of the surfaces of two Al_2O_3 layers (having thicknesses of 5 nm and 200 nm) functionalized with arrays of both SAMs (produced by a combination of microcontact printing and immersion). The difference between the electrostatic potentials produced by the two SAMs (indicated by the line profiles) is about 0.6 V on both substrates, independent of the thickness of the gate oxide. To our knowledge, this is the first experimental confirmation of the often-made assumption that the electrostatic potential of a SAM is not affected by the thickness of the oxide underneath the SAM.

(We note that the potential difference obtained here is significantly smaller than the potential difference reported in Figure 3. This discrepancy is possibly related to the fact that the experiment illustrated in Figure 3 was performed on SAMs that were obtained by immersion of the substrates into a solution of the phosphonic acid, while one of the SAMs investigated here was produced by microcontact printing, which may lead to a less densely packed monolayer compared with the immersion method.)

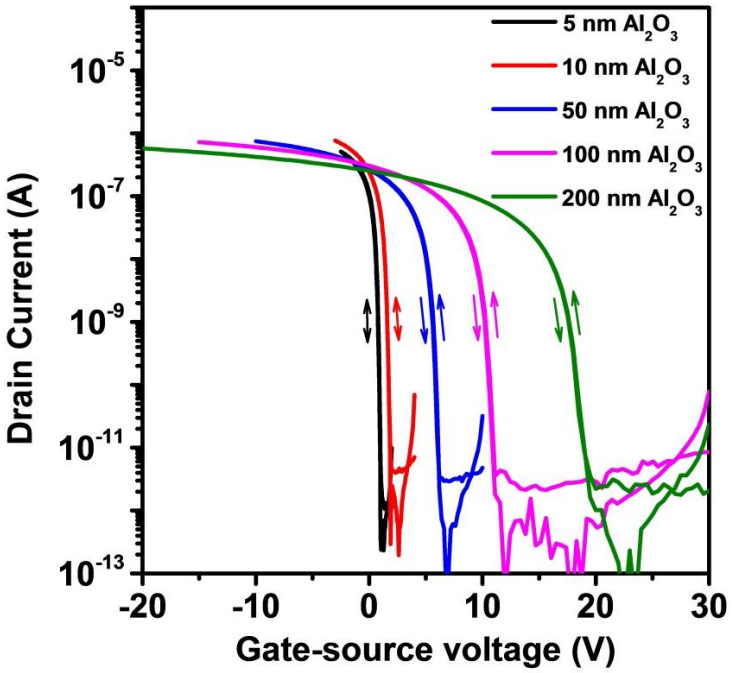

Figure S5. Measured transfer characteristics (forward and backward sweeps) of the DNTT TFTs based on 5 different dielectric thicknesses functionalized with the FC_{18}-PA SAM. Since hysteresis in organic TFTs is often associated with charge-carrier trapping in shallow traps in the semiconductor close to the dielectric interface or with mobile ions in the semiconductor or in the gate-dielectric,[1] hysteresis-free transfer characteristics provide an indication of the absence of such effects.

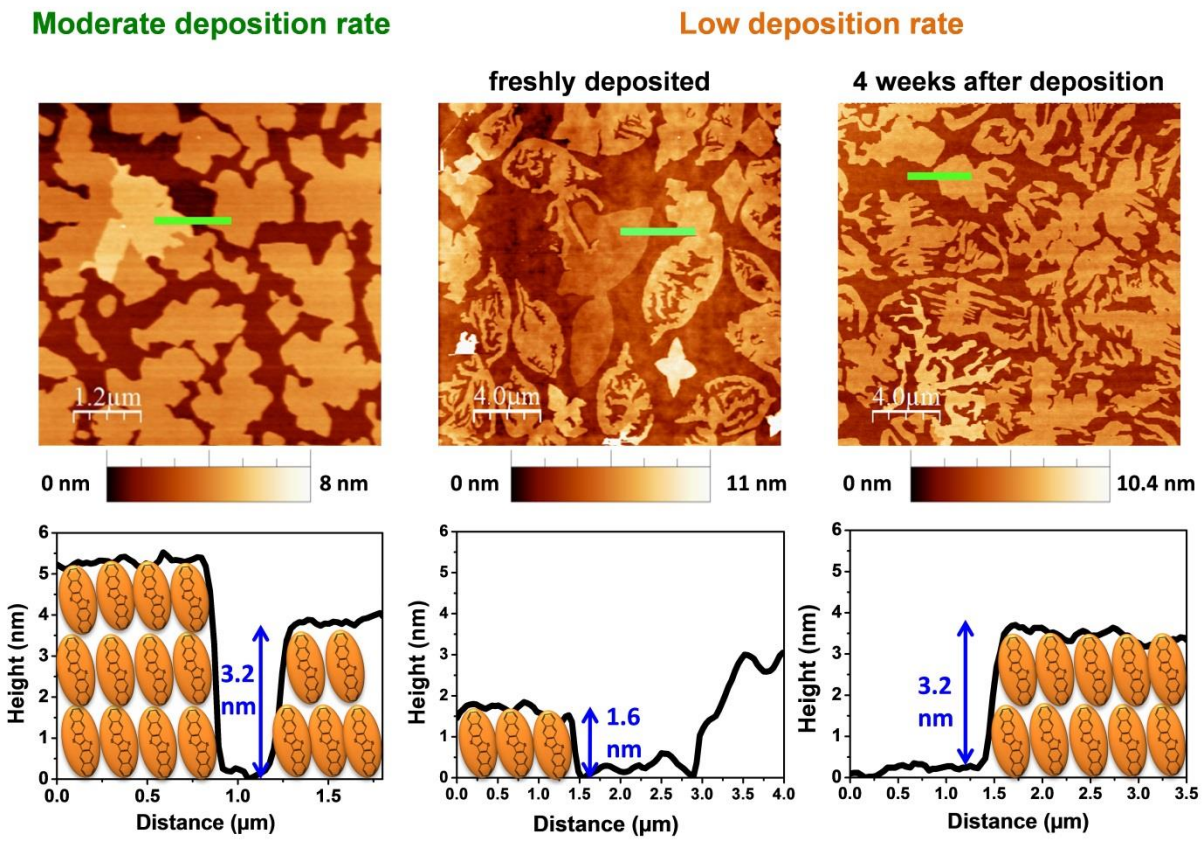

Figure S6. AFM topography images of DNTT layers with a partial surface coverage (nominal thickness 2 nm, indicated by a quartz microbalance) deposited onto an alkyl SAM using deposition rates of 0.03 nms^{-1} and 0.007 nms^{-1}. As can be seen, a moderate deposition rate (0.03 nms^{-1}) leads to the formation of compact islands with a thickness of two or three molecular layers (left), whereas a small deposition rate (0.007 nms^{-1}) produces fractured islands with a thickness of 1.6 nm (which corresponds to one molecular layer),[2] in addition to islands with a thickness of about 10 nm (center).

The topography of the DNTT layer deposited with the low deposition rate (0.007 nms^{-1}) was measured again 4 weeks after fabrication (right). During these 4 weeks, the substrate had been stored in ambient air at room temperature. It appears that the morphology of the DNTT layer evolved during this time, with an apparent trend of a rearrangement of islands that initially had a thickness of one molecular layer (or several molecular layers) into islands with a thickness of exactly two molecular layers. This suggests that single DNTT layers are dynamically unstable and that some molecules climb to form a bilayer, which appears to be a more stable structure for DNTT. This effect has been previously reported by the Frisbie group.[3]

References

(1) Egginger, M.; Bauer, S.; Schwödiauer, R.; Neugebauer, H.; Sariciftci, N. S. Current Versus Gate Voltage Hysteresis in Organic Field Effect Transistors. *Monatsh. Chem*. **2009**, *140*, 735–750.

(2) Yamamoto, T.; Takimiya, K. Facile Synthesis of Highly π-Extended Heteroarenes , Application to Field-Effect Transistors. *J. Am. Chem. Soc.* **2007**, *129*, 2224–2225.

(3) Wu, Y.; Haugstad, G.; Frisbie, C. D. presented at 2013 MRS Spring Meeting, Strain-driven Recrystallization of DNTT Thin Films Observed by Scanning Probe Microscopy, San Francisco CA, April, 2013